

A generalized wall-pressure spectral model for non-equilibrium boundary layers

Saurabh Pargal^{1,2}, Junlin Yuan¹† and Stephane Moreau²

¹Michigan State University, Michigan, USA

²Université de Sherbrooke, Quebec, Canada

1 This study uses high-fidelity simulations (DNS or LES) and experimental datasets to
2 analyse the effect of non-equilibrium streamwise mean pressure gradients (adverse or
3 favourable), including attached and separated flows, on the statistics of boundary layer
4 wall-pressure fluctuations. The datasets collected span a wide range of Reynolds numbers
5 (Re_θ from 300 to 23,400) and pressure gradients (Clauser parameter from -0.5 to 200).
6 The datasets are used to identify an optimal set of variables to scale the wall-pressure
7 spectrum: edge velocity, boundary layer thickness, and the peak magnitude of Reynolds
8 shear stress. Using the present datasets, existing semi-empirical models of wall-pressure
9 spectrum are shown unable to capture effects of strong, non-equilibrium adverse pressure
10 gradients, due to inappropriate scaling of wall pressure using wall shear stress, calibration
11 with limited types of flows, and dependency on model parameters based on friction
12 velocity, which reduces to zero at the detachment point. To address these short-comings,
13 a generalized wall-pressure spectral model is developed with parameters that characterize
14 the extent of the logarithmic layer and the strength of the wake. Derived from the local
15 mean streamwise velocity profile, these two parameters inherently carry effect of the
16 Reynolds number, as well as those of the non-equilibrium pressure gradient and its
17 history. Comparison with existing models shows that the proposed model behaves well
18 and is more accurate in strong-pressure-gradient flows and in separated-flow regions.

19 **Key words:**

† Email address for correspondence: junlin@msu.edu

1. Introduction

The fluctuation in space and time of the wall pressure beneath a turbulent boundary layer is one of the major sources of flow-induced noise and vibrations. Accurate modeling of the statistics of wall-pressure fluctuations is important for noise prediction in a wide range of applications such as wind turbines (??), cooling fans (??), propellers (?), unmanned/manned air vehicles or drones (??), and cabin noise (?), etc., as well as for prediction of flow-induced structure fatigue (?). In these applications, the boundary layer flows are often turbulent and non-equilibrium, due to surface curvature and significant pressure gradients that vary in the streamwise direction, which may induce boundary layer separation and can be found in a large range of Reynolds number. Here, a non-equilibrium boundary layer is defined as that with streamwise (i.e. x) variation of the Clauser parameter, $\beta(x) = (\delta^*/\tau_w)(dp_e/dx)$, where $\delta^*(x)$ is the displacement thickness, $\tau_w(x)$ is the wall shear stress, and $p_e(x)$ is the static pressure at the edge of the boundary layer. Therefore, the generation of noise in non-equilibrium turbulent boundary layers is physically complex and challenging to model.

The modeling of wall-pressure loading as a noise source predominantly depends on the power spectral density (PSD) of wall-pressure fluctuations, as well as its spanwise correlation length and the convection velocity of turbulent structures (????). The focus here is on modeling wall-pressure spectrum (WPS). It is established that the WPS of a boundary layer with zero or minimal pressure gradient consists of three ranges (??): (i) a range with ω^2 variation at low frequencies (where ω is the frequency), (ii) a range with ω^{-5} behavior at high frequencies, and (iii) an overlap range with an approximate ω^{-1} decay between the above two ranges. Based on data primarily in equilibrium flows, the width of the overlap range was found to increase with Reynolds number (?).

Contributions from different layers of wall turbulence to the WPS has been studied and are summarized below. The experimental studies of ? suggested different dominant sources for different wavenumber ranges of the WPS: the high-wavenumber range

is mainly attributed to turbulent activities in the logarithmic region, while the low-wavenumber range is attributed to large-scale turbulent motions in the outer layer. ? quantified the correlations between the fluctuations of wall pressure and those of streamwise velocity in different layers of boundary layer and observed that high-frequency and overlap ranges of the WPS are associated with flows in the buffer and logarithmic regions, respectively. As opposed to earlier studies performed on channel flow or canonical flat-plate boundary layer data, ? analyzed data collected near the trailing edge of a cambered aerofoil with a strong mean adverse pressure gradient (APG) in a highly non-equilibrium turbulent boundary layer, to compare contributions from various velocity sources (i.e. the mean-shear and turbulence-turbulence terms) at different wall-normal locations to the wall-pressure fluctuations based on the pressure Poisson's equation. They found that the mean shear (MS) term in the inner and logarithmic regions is the dominant contributor, especially in the mid-to-high frequency range.

Past studies were mostly on zero-pressure-gradient (ZPG) turbulent boundary layers. They showed that the wall-pressure fluctuations (evaluated by the root-mean-square values, p_{rms}) are amplified under a higher Reynolds number, mainly due to the increase in overlap-range spectral contribution. For a ZPG flat-plate boundary layer, ? integrated the pressure spectrum over various frequency ranges and showed that the low-to-mid frequency range and the high-frequency range were not sensitive to a change in Reynolds number, whereas the significance of the overlap range increases with Reynolds number, leading to an augmentation of p_{rms} . They proposed that $p_{rms}^2/\tau_w^2 = 6.5 + 1.86 \ln(Re_\tau/333)$, which was tested with ZPG boundary layer and channel flow data. ? also demonstrated that the overlap range is correlated with the Reynolds number.

The current understanding of the WPS in non-zero pressure gradient flows is summarized as follows. Review of the earlier work before the mid 1990s are provided by ? and ?. ? showed that under an APG low-frequency contents of the WPS become more prominent as large eddies are energized, while the high-frequency contents become less important. Under a favourable pressure gradient (FPG), however, the opposite applies, with stronger high-frequency contents. The WPS slope in the overlap range also varies with the pressure gradient. ? investigated the effects of mild pressure gradient using

77 large-eddy simulations (LES) and showed scale-based dependencies of the WPS on FPG
 78 similar to those observed before. ? conducted direct numerical simulation (DNS) of a
 79 boundary layer with prescribed freestream suction and blowing to induce flow separation
 80 and reattachment. They showed that none of the outer, inner or mixed scaling collapsed
 81 the wall-pressure spectra in all regions of the flow. Normalisation with the local maximum
 82 magnitude of the Reynolds shear stress, however, was shown to collapse the low-frequency
 83 range of WPS for APG flows including those with separation (???)

84 Modeling of turbulent WPS is broadly classified in two categories: (i) semi-empirical
 85 modelling and (ii) analytical modeling based on solution of the Poisson’s equation of
 86 pressure (??????). The focus of this paper is on the first approach, which requires a
 87 smaller amount of inputs from the flow field in comparison to the analytical modelling
 88 approach. Existing semi-empirical WPS closures mostly model the magnitude and shape
 89 of the WPS normalized by some boundary-layer parameters that are either internal,
 90 external or mixed, such as the boundary layer thickness (δ), the edge velocity (U_e) and
 91 the wall shear stress ($\tau_w = \rho u_\tau^2$, where u_τ is the friction velocity and ρ is the density),
 92 etc. For some of these studies see ?, ?, ?, ?, ?, ?, ?, ?, ?, ?, and ?. ? proposed a
 93 model for ZPG boundary layers, which accurately models the Reynolds number effect
 94 on the wall-pressure spectrum for these flows. To capture the pressure gradient effect,
 95 several other models have been proposed (??????). ? integrated additional boundary
 96 layer flow parameters to sensitize the model to pressure gradient effects, especially
 97 those of APG. The additional parameters include Clauser’s parameter (β) (?) and
 98 Cole’s wake parameter (II) (?). The former includes the local effect of mean pressure
 99 gradients, while the latter represents the cumulative effect of the history of mean pressure
 100 gradient up to the considered location in the boundary layer. Several later models
 101 developed modifications of the model that capture effects of other complexities such
 102 as wall curvature and FPG. ? developed a model by fitting it on a large amount of
 103 experimental WPS data collected in various non-equilibrium boundary layer flows on
 104 aerofoils. ? used the shape factor (H) and Reynolds numbers (Re_θ or Re_τ) instead of β
 105 to incorporate the effect of non-equilibrium pressure gradients, as β — a descriptor of
 106 local pressure gradient — does not carry the history effect of a spatially varying pressure

107 gradient. ? improved Rozenberg’s model based on experimental data gathered from a
108 wide range of flows with different Reynolds numbers and pressure gradients. ? proposed
109 a new model for flows with FPG. Recently, machine learning approaches such as gene
110 expression programming and artificial neural networks were used to model WPS as a
111 function of boundary layer parameters (????).

112 Despite the success of the models mentioned above in the specific flows for which
113 they were developed, these models are not universally applicable to both ZPG flows
114 and those with non-equilibrium pressure gradients and/or surface curvature, due to
115 the following reasons. (i) Models developed by curve-fitting to data of a limited type
116 of flows do not naturally apply to other flows, such as Goody’s model, which works
117 for ZPG flows only. (ii) Normalisations of wall-pressure statistics used for ZPG flows
118 (e.g. τ_w) may not be appropriate for strong-APG flows (e.g. a boundary layer close to
119 separation where τ_w approaches zero). (iii) The choices of local boundary layer parameters
120 do not account sufficiently for the history effect of the pressure gradient. In addition,
121 some existing models were developed based on experimental wall-pressure measurements
122 that are supplemented with low-fidelity flow-field data, such as those estimated from
123 XFOIL (?).

124 The objective of this study is therefore to develop a general WPS model that is
125 tunable for both ZPG and non-equilibrium, strong-pressure-gradient turbulent boundary
126 layers, as well as special cases such as flow separation and reattachment. To this end,
127 model parameters that capture the local characteristics of the mean streamwise velocity
128 profile (which evolves under a history of the pressure gradient variation) are derived and
129 incorporated to sensitize the model to the streamwise pressure gradient and its history.
130 An appropriate pressure normalisation for flows with and without pressure gradients is
131 used. The model is calibrated based on a large and inclusive database, containing both
132 experimental measurements and DNS/LES data (existing or new) of flows over a wide
133 range of Reynolds number, with or without separation.

134 The organization of the paper is as follows. Section ?? describes the database, Sec-
135 tion ?? presents the boundary layer development of the cases in the datasets, Section ??
136 discusses the wall-pressure fluctuations and WPS in the datasets, Section ?? discusses

Cases	Re_θ	β	$K(10^6)$
?, DNS	300-1200	0 to 12	-4 to 0
?, DNS	300-1200	0 to 10	-4 to 0
?, DNS	300-1300	-	-1.4 to 1.0
?, LES	2100-7000	-	-25 to 25

TABLE 1. List of simulation datasets. For the cases of ? and ?, the boundary layer separation leads to β values between $-\infty$ and ∞ . The Reynolds number values are slightly different from those in ? and ? due to difference in the definitions of the boundary layer edge.

137 the performances of existing WPS models and then introduces a new generalized WPS
 138 model, and conclusions are presented in Section ??.

139 2. Datasets collection

140 The first step to develop a generalized WPS model is to collect and analyze high-fidelity
 141 datasets in a wide range of flows. The goal is to collect datasets for both equilibrium
 142 and non-equilibrium boundary layers, including ZPG, FPG, and APG flows, with or
 143 without wall curvature (as in boundary layers developed on aerofoils) and boundary
 144 layer separation and reattachment, across a wide range of Reynolds number based on
 145 momentum thickness ($Re_\theta = 300$ to 23,400).

146 2.1. Simulation datasets

147 DNS and LES datasets are gathered or re-generated from cases in four prior studies:
 148 ?, ?, ? and ?. Details of the flows in these datasets are listed in Table ??. The first
 149 three are DNS while ? is a LES study. The data of ? and ? are collected directly from
 150 simulations of turbulent boundary layer on a flat-plate and that on a controlled-diffusion
 151 (CD) aerofoil with matched non-equilibrium APG distributions along the streamwise
 152 direction. Comparison between these two flows reveal the effects of the convex wall
 153 curvature and the trailing edge on WPS, which were partially discussed in ? and will
 154 be further discussed for the WPS herein. ? and ? conducted simulations of flat-plate
 155 boundary layers with suction and blowing freestream velocities, leading to boundary layer
 156 separation and then reattachment; these two cases are rerun to collect boundary layer
 157 parameters, streamwise mean velocity and wall-pressure statistics at the same streamwise

158 locations, as these data were not fully available from the original publications. For the
159 case of ?, this work provides new data as the wall pressure was not discussed previously.

160 A brief summary of the four simulations is as follows. The case of ? provides DNS data
161 on a boundary layer developing on the pressure side of a CD aerofoil, at a freestream Mach
162 number of 0.25. The compressible Navier-Stokes equations are solved for the flow around
163 an aerofoil with the multi-block structured code HiPSTAR (High Performance Solver for
164 Turbulence and Aeroacoustics Research) (?). An initial 2D RANS simulation was run to
165 provide boundary and initial conditions to the DNS simulation. Details of the problem
166 formulation are provided by ?. The simulation was validated against experimental data
167 (??) for wall-pressure spectral data and flow statistics at different streamwise locations.
168 The case of ? is an incompressible DNS of a flat-plate turbulent boundary layer to
169 emulate the boundary layer development on the downstream portion of the CD aerofoil
170 flow studied by ?. A finite difference solver on a staggered grid was used. To match the
171 pressure gradient parameter (K) of the aerofoil boundary layer, a streamwise pressure
172 gradient was imposed by prescribing a streamwise-varying $U_\infty(x)$ at the top boundary
173 of the domain. A fully turbulent boundary layer flow at the inlet of the domain was
174 obtained using the recycling/rescaling method. A convective outflow boundary condition
175 was used at the outlet and periodic boundary conditions are used in the spanwise
176 direction. Similar discretization methods and boundary conditions were used in ? and ?
177 with slight variations in details. Simulations of the flows in these two studies were rerun,
178 based on the methodologies of ?. The meshes in the new simulations were similar to those
179 in the original studies. The same domain lengths and similar boundary conditions were
180 used. The rerun simulation of ? has been validated against results reported in the original
181 work on flow statistics and wall-pressure spectra at different streamwise locations. For the
182 rerun LES simulation of ?, the governing equations were solved for the filtered velocities
183 at scales larger than the low-pass filter. A different dynamic eddy-viscosity model based
184 on the Lagrangian-averaging procedure (?) was used for the present simulation. Boundary
185 layer developments in the rerun simulations will be compared to those reported in the
186 original studies in Section ??.

2.2. Experimental datasets

DNS and LES simulations are limited to comparatively low Reynolds numbers ($Re_\theta=300$ to 7000). Experimental datasets are gathered from the studies of ?, ?, and ?, which provide ZPG or pressure-gradient flow data with Re_θ of up to 23,400. Only existing datasets with both mean velocity profile data and WPS data measured at the same streamwise locations are included, as these quantities are required to calibrate and test the proposed model to be introduced in Section ??.

A brief description of the experimental setup of each case is given below. ? carried out experiments in an open-jet anechoic test section of Acoustic Wind Tunnel Braunschweig (AWB). Adverse and favorable pressure gradients in flat-plate boundary layers were achieved by placing a rotatable NACA 0012 aerofoil above the flat plate. Wall-pressure statistics were measured with sub-miniature pressure transducers and boundary layer velocity profiles were obtained using hot wires. Re_θ was up to 19,000, with $\beta = -0.9$ to 16. The study is among the few experimental studies that measured wall-pressure statistics across very different flows due to the very wide ranges of pressure gradient and Reynolds number. Similarly, ? carried out experiments in a subsonic wind tunnel with a NACA 0012 aerofoil installed in the center of the test section. The boundary layer was tripped at the upstream section, to ensure a fully turbulent boundary layer in the test section. Wall-pressure statistics were measured for non-equilibrium pressure gradients ranging from β of -0.5 to 0.5 , with Re_θ reaching 18,000. ? carried out measurements in the boundary-layer tunnel of the Aerospace and Ocean Engineering department of Virginia Tech. The wall-pressure statistics measurement was limited to ZPG flows but data reached Reynolds numbers as high as $Re_\theta = 23,400$.

3. Boundary layer development

In this section, the streamwise developments of pertinent flow and boundary layer variables are presented for cases in the database. The goal is to provide insights on the appropriate choice of scaling variables for WPS modeling in non-equilibrium flows. The various boundary layer variables presented here are used as input parameters in several existing wall-pressure spectral models to normalize the spectrum and to model the effects

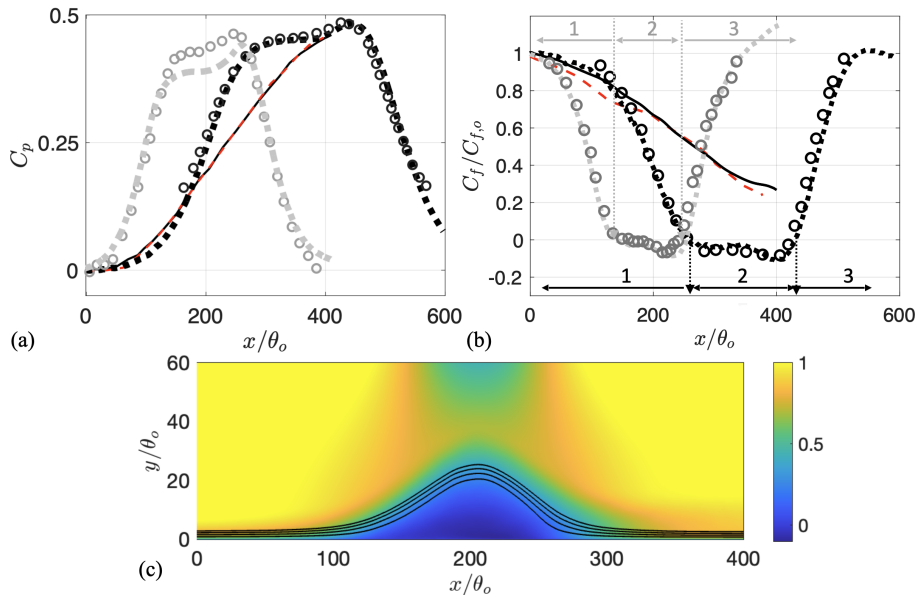


FIGURE 1. (a) Pressure coefficient and (b) friction coefficient in ? (—), ?(---), ? (---) and ? (---), compared to original data of ? and ? (o). (c) Contours of mean streamwise velocity normalized by U_e (at the reference location) in ? case, with streamlines shown at stream-function values of $\psi_o = 0.5, 1, 1.5$ and 2.

216 of Reynolds number and pressure gradient. This section helps understand why some WPS
 217 models give large errors in strong-pressure-gradient flows; it also provides insights on
 218 better choices of input parameters and scaling variables in modeling the WPS for these
 219 flows. First, Figures ?? to ?? discuss the boundary layer development for the continuous
 220 streamwise location range for the simulated cases. Then the experimental datasets are
 221 discussed at discrete streamwise locations, as the data were only available there. Here,
 222 the streamwise, wall-normal and spanwise directions are denoted as x, y and z . u, v and
 223 w are the velocity components in those directions, p is the static pressure, and t is time.
 224 An instantaneous flow variable $\phi(x, y, z, t)$ is decomposed as $\phi = \overline{\phi}(x, y) + \phi'(x, y, z, t)$,
 225 where $\overline{(\cdot)}$ denotes averaging in z and time.

226 Figure ?? shows the variation of the mean wall-pressure coefficient, $C_p = (\overline{p}|_{y=0} -$
 227 $p_{e,o})/(0.5\rho U_e^2)$, and skin friction coefficient, $C_f = (u_\tau/U_e)^2/2$, where $p_{e,o}$ is edge static
 228 pressure at the location of $x = 0$, which corresponds to the reference (ZPG) location
 229 defined in each of the studies. In Figure ??(b), the C_f is normalized by its value at the
 230 reference location to better compare all cases. Only simulated cases are presented as the
 231 boundary-layer parameters for a continuous range of x are available. Figures ??(a) shows

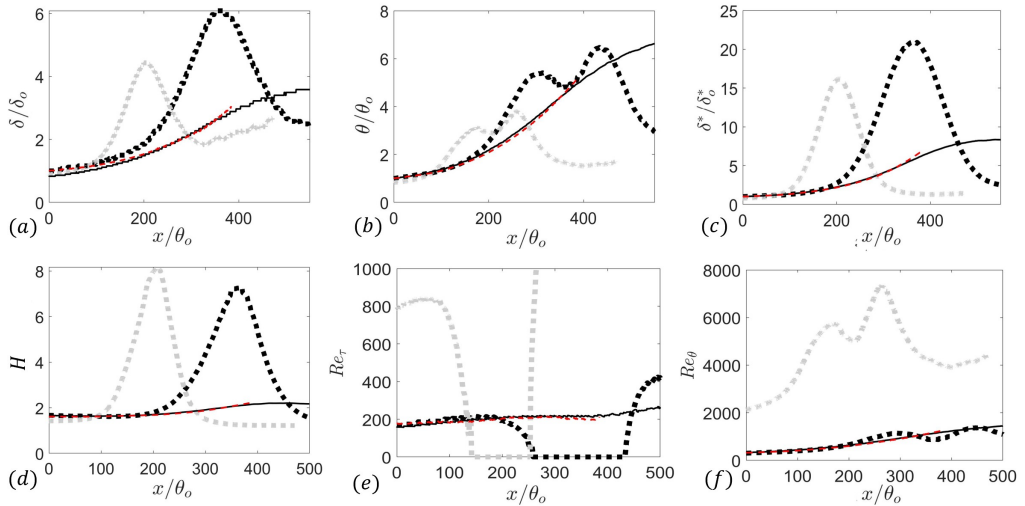


FIGURE 2. Boundary layer parameters in ? (—), ? (---), ? (···) and ? (-·-·).

232 that the variations of C_p in the flat-plate (?) and aerofoil (?) cases are very similar. In
 233 Figures ??(b), the variations of C_f are shown to match overall for these two cases, with
 234 some differences due to the convex wall curvature and trailing-edge effects (?). These
 235 comparisons are discussed in ?, showing that the convex curvature on the pressure side
 236 of the aerofoil does not lead to significant changes in C_p and C_f . In the cases of ? and
 237 ? where the flows undergo freestream suction and blowing, the C_p variation indicates
 238 three phases of a separated boundary layer flow (marked in Figures ??(b)): (1) attached
 239 APG flow, (2) separated region and (3) reattached flow under FPG. This is also reflected
 240 in C_f variations: C_f first decreases toward zero in the APG region, reaching negative
 241 values in the separated flow region, and increases near the flow reattachment in the FPG
 242 region. The fact that C_f reaches zero in separated flows suggests that the use of τ_w to
 243 non-dimensionalize the pressure in some existing WPS models is problematic in these
 244 flows. The contour of mean streamwise velocity of the case of ? in Figure ??(c) confirms
 245 these flow stages. The coefficients are compared between the results of the present rerun
 246 simulations and those of the original studies (??); good match is obtained in both cases.
 247 The difference in C_p values near $x/\theta_o \approx 200$ in the ? data in Figure ??(a) is due to the
 248 different definitions of the boundary layer edge employed in the present study and that
 249 in the original study.

250 In Figure ??, the variations of boundary-layer thickness (δ), momentum thickness

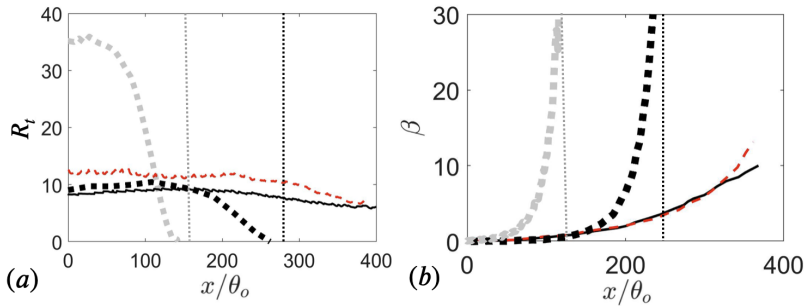


FIGURE 3. Development of R_t and β in ? (—), ? (---), ? (---) and ? (---). For ? and ? cases, only the attached-flow region upstream of the separation point is shown; --- (vertical): location of separation point.

251 (θ) and displacement thickness (δ^*) along the streamwise direction are shown. These
 252 thicknesses are used as inputs in several existing wall-pressure spectral models. As
 253 expected with an increase in APG, the boundary layer becomes thicker. For the cases with
 254 suction and blowing, the thicknesses reach their maxima near the end of the APG zone
 255 and then decrease with FPG. The development of the shape factor, H , in Figure ??(d)
 256 shows a similar response, which reflects that the displacement thickness is more sensitive
 257 to the pressure gradients compared to the momentum thickness. Reynolds numbers based
 258 on different velocity scales that have been used in some wall-pressure spectral models
 259 are also compared. The one based on the inner velocity, $Re_\tau = u_\tau \delta / \nu$ (where ν is the
 260 kinematic viscosity), shows a similar trend as that of C_f (Figure ??(e)), while the one
 261 based on edge velocity, $Re_\theta = U_e \theta / \nu$, shows a variation similar to that of θ (Figure ??(f)).
 262 The DNS cases are conducted in low Reynolds numbers ($Re_\theta \approx 300$ to 1200), while higher
 263 values are reached for the LES case ($Re_\theta \approx 2000$ to 7000).

264 Figure ?? shows the streamwise developments of two boundary layer parameters
 265 that are used in most existing WPS models to sensitize the modelled spectrum to the
 266 Reynolds number and the pressure gradient: $R_t \equiv Re_\tau(u_\tau/U_e)$ (Figure ?? (a)) and β
 267 (Figure ?? (b)), respectively. As the separation point is approached, R_t tends to 0 and β
 268 to infinity. This indicates issues in many existing WPS models when used for strong-APG
 269 flows near incipient separation (?), which are examined in detail in Section ??.

270 For most of the experimental datasets, streamwise variations of the boundary layer
 271 parameters are available at discrete locations only. Representative values of Re_θ , H , C_f
 272 and β are tabulated in Table ??. Specifically, the datasets of ? experiments contain five

Cases	Re_θ	H	C_f	β
?, ZPG	4889	1.41	0.0025	0
?, APG (-6°)	6979	1.61	0.0017	3.8
?, APG (-10°)	8670	1.75	0.0012	6
?, APG (-14°)	11046	2.12	0.0006	12.5
?, FPG (14°)	1940	1.26	0.0068	-0.5
?, ZPG (2°)	16000	1.29	0.0026	-0.02
?, APG (12°)	18606	1.31	0.0024	0.58
?, FPG (-10°)	14000	1.26	0.0028	-0.47
?, ZPG	7300	1.29	0.0026	0
?, ZPG	23400	1.29	0.0022	0

TABLE 2. List of experimental datasets and values of boundary layer parameters at measurement locations of available data. For ? and ? datasets, the angle of attack of the aerofoil imposed to generate mean pressure gradient is indicated.

273 cases: one ZPG flow, three APG flows with β varying from 4 to 12, and one FPG flow, at
274 $Re_\theta = 5,000$ to 11,000. The data show that boundary layer thicknesses (as indicated here
275 by Re_θ ; for other thicknesses see the original studies) and the shape factor increase with
276 APG and decrease in FPG, whereas C_f decreases with APG and increases in FPG. The
277 cases from ? are non-equilibrium APG and FPG flows but with comparatively milder
278 APG compared to ?. As a result, the variations in boundary layer parameters are more
279 limited. Also included are measurements by ?, which were carried out for ZPG flows only
280 but reached higher Reynolds numbers.

281 4. Wall-pressure statistics

282 In this section, the development of wall-pressure statistics along x is discussed using the
283 datasets. Different normalisations are used to analyze the wall-pressure scaling. Effects
284 of pressure gradient, boundary layer separation and reattachment on the wall-pressure
285 spectrum are examined. The goal is to (1) identify the appropriate scalings to be used in
286 the WPS model for attached and separated flows and (2) examine the changes of WPS
287 due to strong pressure gradients or separation, which will be shown to be well predicted
288 by the new model in Section ??.

289 The streamwise variations of the root-mean-square (r.m.s.) of wall-pressure fluctuations
290 and the local maximum magnitude of the Reynolds shear stress profile ($|\overline{u'v'}|_{\max}$) are

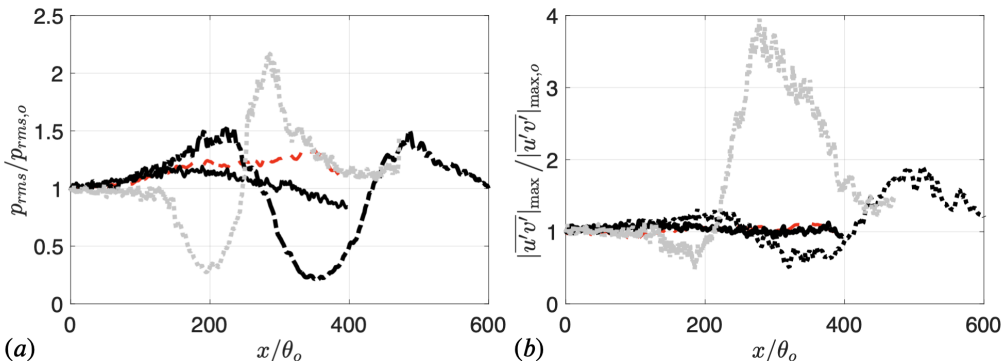


FIGURE 4. (a) Wall-pressure r.m.s. normalized by its value at the reference location and (b) local peak magnitude of Reynolds shear stress, normalized by its value at the reference location, in ? (—), ? (---), ? (···) and ? (-·-·).

291 compared in in Figures ??(a) and ??(b), respectively. Both quantities are normalized
 292 by their specific values at $x = 0$. Only numerical data are shown as, for experimental
 293 datasets, $p_{rms}(x)$ and $|\overline{u'v'}|_{\max}(x)$ are not available. Convex wall curvature and trailing-
 294 edge effect (?) intensify the wall-pressure fluctuations, as shown by the comparison
 295 between the flat-plate case of ? and the aerofoil case of ? for $x/\theta_o > 200$. In the separated-
 296 flow region, a drop in wall-pressure fluctuations is seen, which was also observed by ?.
 297 The dip is attributed to the departure of turbulent eddies from the wall, with mainly
 298 large recirculating eddies interacting with the near-wall region. As the separated shear
 299 layer reattaches, the re-emergence of intense turbulent motions near the wall leads to
 300 an augmentation of wall-pressure fluctuations, shown by the $p_{rms}(x)$ maximum shortly
 301 after the reattachment point (at $x/\theta_o \approx 280$ for ? and $x/\theta_o \approx 500$ for ?). Interestingly,
 302 Figure ??(b) shows that the x variation of the local maximum magnitude of the Reynolds
 303 shear stress profile, $|\overline{u'v'}|_{\max}(x)$, is very similar to that of p_{rms} : the decrease near the
 304 separation point and the peak near the flow reattachment occur at almost the same
 305 x locations downstream from the reattachment point, as the flow recovers towards the
 306 equilibrium ZPG flow, both p_{rms} and $|\overline{u'v'}|_{\max}$ reduce towards the ZPG values at $x = 0$.
 307 To identify the best pressure scale to be used in a WPS model for strong-pressure-
 308 gradient flows, in Figure ?? different quantities are used to normalize wall-pressure r.m.s.
 309 as it varies along x , for the datasets shown in Figure ??. The r.m.s. normalized by τ_w
 310 (Figure ??(a)) increases with APG and tends towards infinity as the separating point

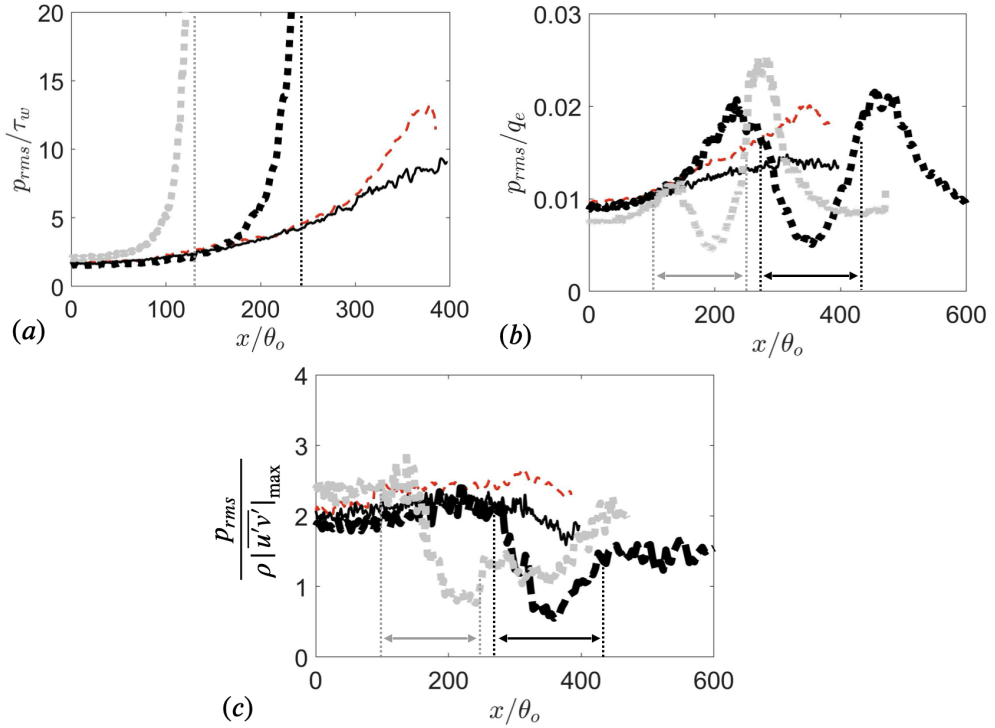


FIGURE 5. Wall-pressure r.m.s. normalized by (a) local wall shear stress (τ_w), (b) local dynamic pressure (q_e), and (c) local peak magnitude of Reynolds shear stress. In (a), --- (vertical): locations of separation points. In (b) and (c), separated-flow regions are marked. Datasets include ? (—), ? (---), ? (· · ·) and ? (· · ·).

311 is approached. The use of τ_w to scale p_{rms} in WPS models is, therefore, inappropriate
 312 for strong-APG boundary layers. The r.m.s. normalized by $q_e = 0.5 \rho U_e^2$ (Figure ??(b))
 313 displays a significant increase in the APG zone before the flow separation. This is because
 314 wall-pressure fluctuations are augmented in the APG region, while the edge velocity
 315 decreases. In comparison, $p_{rms}/(\rho|\overline{u'v'}|_{max})$ stays almost constant as long as the boundary
 316 layer is attached, regardless of the pressure gradient (Figure ??(c)). In the separated flow
 317 regions, however, a dip of $p_{rms}/(\rho|\overline{u'v'}|_{max})$ is observed, caused by a faster damping of
 318 p_{rms} inside the recirculation bubble than that of the Reynolds shear stress in the detached
 319 shear layer (as shown in Figure ??). These observations indicate that wall-pressure r.m.s.
 320 scales better with $\rho|\overline{u'v'}|_{max}$ than with q_e or τ_w , in attached flows under strong pressure
 321 gradients, suggesting that the wall pressure fluctuation magnitude is closely correlated
 322 with active turbulent motions and that $\rho|\overline{u'v'}|_{max}$ should be used as the pressure scale in
 323 a WPS model; similar observations were made by ?, ? and ?. However, the appropriate

Cases	Legend
?, $x/\theta_o = 0$, ZPG ($\beta = 0$)	—
?, $x/\theta_o = 100$, Low APG ($\beta = 0.3$)	—
?, $x/\theta_o = 290$, APG ($\beta = 5$)	—
?, $x/\theta_o = 340$, High APG ($\beta = 8$)	—
?, $x/\theta_o = 0$, ZPG ($\beta = 0.01$)	---
?, $x/\theta_o = 100$, Low APG ($\beta = 0.28$)	---
?, $x/\theta_o = 290$, APG ($\beta = 4.8$)	---
?, $x/\theta_o = 340$, High APG ($\beta = 8.3$)	---
?, $x/\theta_o = 50$, Low APG ($\beta = 0.9$)	—
?, $x/\theta_o = 105$, Very high APG ($\beta = 22.8$)	—
?, $x/\theta_o = 120$, Very high APG ($\beta = 46.28$)	—
?, $x/\theta_o = 130$, Before flow separation ($\beta = 171$)	—
?, $x/\theta_o = 50$, ZPG ($\beta = 0.018$)	—
?, $x/\theta_o = 210$, High APG ($\beta = 8$)	—
?, $x/\theta_o = 230$, Before flow separation ($\beta = 162$)	—
?, ZPG ($\beta = 0.1$)	○
?, High APG (-10°) ($\beta = 6$)	●
?, Very high APG (-14°) ($\beta = 12.5$)	●
?, FPG (14°) ($\beta = -0.5$)	○
?, ZPG (2°) ($\beta = 0$)
?, APG (12°) ($\beta = 0.5$)
?, FPG (-10°) ($\beta = -0.5$)
?, ZPG (7300) ($\beta = 0$)
?, ZPG (23400) ($\beta = 0$)

TABLE 3. Datasets in attached-flow regions (under ZPG, APG or FPG) that are considered in analyses of wall-pressure spectrum.

324 wall-pressure r.m.s. scaling for the separated flow region remains yet to be found; but
325 this is out of the scope of the present work.

326 The PSD of the wall-pressure fluctuations (denoted by ϕ_{pp}) is computed for all
327 simulated and experimental cases and compared in Figure ???. Only attached-flow regions,
328 with ZPG or non-equilibrium APG, are considered here. The x location, β value, and
329 legend for each PSD curve in Figure ??? are listed in Table ???. Different normalisations
330 are compared. Both Re_θ ($Re_\theta = 300$ to 23,400) and β ($\beta = 0$ to 200) vary greatly
331 among these data. The high β values occur near the separation points. In the following
332 discussion, it will be shown that a robust set of scales to be used for strong-pressure-
333 gradient-flow WPS modeling is $\rho \overline{|u'v'|}_{\max}$ as the pressure scale, δ as the length scale, and

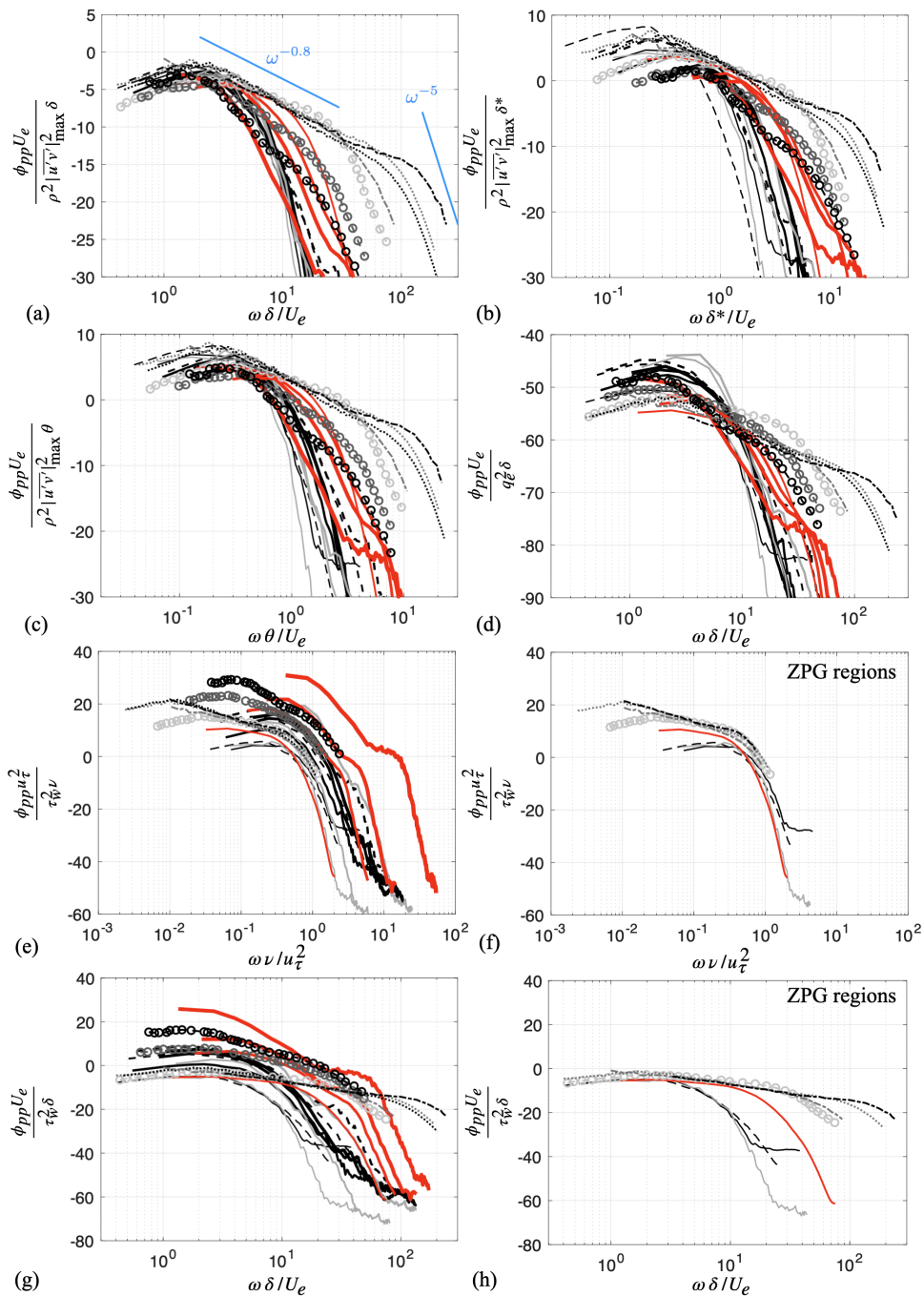


FIGURE 6. (a-c) Power spectral density (PSD) of wall-pressure fluctuations for attached-flow datasets with ZPG and APGs listed in Table ??, under three different scalings involving $\rho|u'v'|_{\max}$ (as the pressure scale) and outer scales: (a) $\rho|u'v'|_{\max}$, δ and U_e , (b) $\rho|u'v'|_{\max}$, δ^* and U_e , and (c) $\rho|u'v'|_{\max}$, θ and U_e . Other normalisations with (d) outer scales (q_e , δ and U_e), (e,f) inner scales (τ_w , δ_ν and u_τ , with ZPG profiles shown separately in (f) demonstrating high-frequency collapse), and (g,h) mixed scales (τ_w , δ and U_e , with ZPG profiles shown separately in (h) demonstrating low-frequency collapse). The PSD is evaluated in dB, defined as $10 \log_{10}(\phi_{pp})$. Legend is listed in Table ??.

334 U_e as the velocity scale.

335 Figure ??(a) compares the results using $\rho|\overline{u'v'}|_{\max}$ as the pressure scale, δ the length
 336 scale, and U_e the velocity scale (or equivalently p_{rms} , δ^* and the Zagarola-Smiths velocity,
 337 as shown by ?). Note that in the experimental datasets the Reynolds shear stress data
 338 were missing. For these experimental datasets, the wall shear stress (τ_w) at a mild-
 339 APG ($\beta < 1$) location immediately upstream of the APG region, instead of the local
 340 Reynolds shear stress, is used to form the pressure scale for the strong-APG region. This
 341 approximation for the experimental datasets is based on the observation that $|\overline{u'v'}|_{\max}(x)$
 342 does not vary significantly in the attached-flow region upstream of the separation point,
 343 as shown previously in Figure ??(b). The value of $|\overline{u'v'}|_{\max}(x) \approx |\overline{u'v'}|_{\max}(0)$ can then be
 344 approximated as $\tau_w(0)$ due to the existence of a constant-stress layer in a boundary layer
 345 under zero or mild pressure gradients. The treatment mentioned above is employed for the
 346 experimental cases only. Under such normalisation, Figure ??(a) shows that approximate
 347 low-frequency collapse is obtained. There is a small spread (within 3 dB for numerical
 348 datasets and within 4 dB to 5 dB for experimental ones); but this is a better low-frequency
 349 collapse as compared to results using other sets of scalings as shown in Figures ??(b-
 350 e,g). The approximate collapse is expected as the low-frequency contents are the main
 351 contributor to p_{rms} , which in turn scales with $\rho|\overline{u'v'}|_{\max}$. Swapping the length scale for δ^*
 352 or θ , however, gives more scatter in the low-frequency range (Figures ??(b) and (c)), as
 353 also shown by ?. Even though previous works (???) have shown $\rho|\overline{u'v'}|_{\max}$ to be the best
 354 pressure scaling for wall-pressure spectra, most of them were limited to low Reynolds
 355 number cases with mild pressure gradients. The comparison here shows that the chosen
 356 set of scaling collapses low-frequency portion of the PSD for a large range of Reynolds
 357 number with strong non-equilibrium APG as well.

358 In addition, Figure ??(a) shows that a strong APG leads to a milder overlap-range
 359 decay rate (as compared to the ZPG rate of around -0.8). In addition, the high-frequency
 360 ω^{-5} relation is shown to apply under a strong APG. The datasets, however, do not reach
 361 a sufficiently low frequency range to examine the APG effect on the ω^2 relation observed
 362 in ZPG flows for $\omega\delta/U_e < 0.1$ (see, for example, ?).

363 Figures ??(e) shows that normalisation based on inner velocity and length scales (i.e.

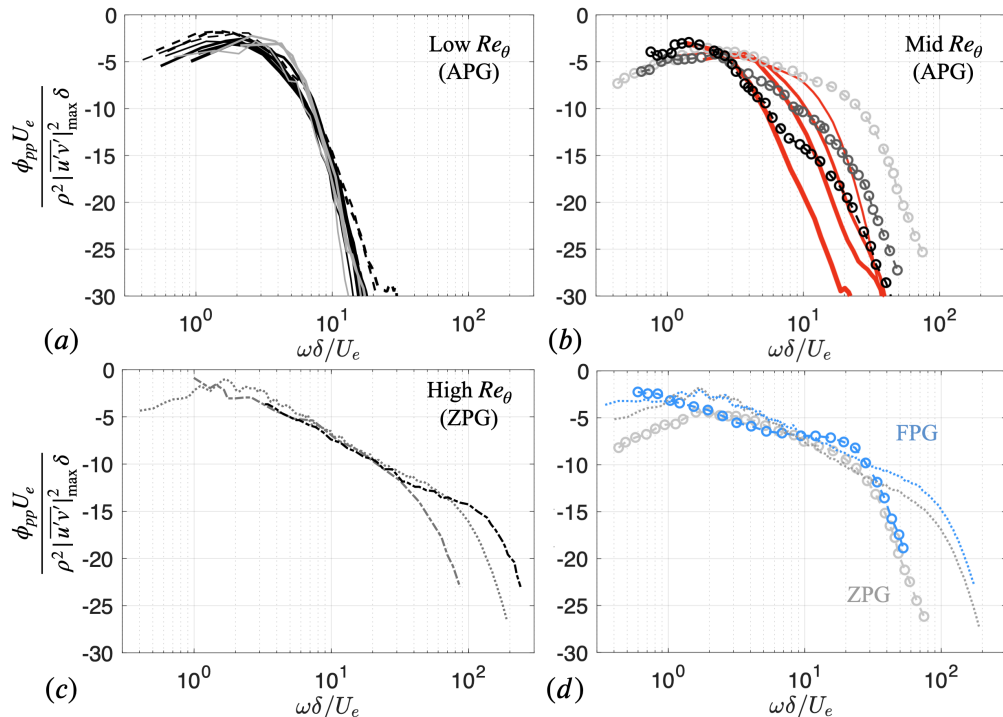


FIGURE 7. Wall-pressure PSDs in APG boundary layers with different Reynolds number ranges: (a) low- Re_θ range ($Re_\theta = 300$ to 1000), (b) mid- Re_θ range ($Re_\theta = 2000$ to 8000), and (c) high- Re_θ range ($Re_\theta = 8000$ to 23400). (d) PSDs in FPG flows (blue) compared to ZPG ones (gray). See Table ?? for legend.

364 using τ_w , $\delta_\nu \equiv \nu/u_\tau$ and u_τ) gives a high-frequency collapse for the ZPG spectra (see
 365 ZPG profiles shown separately in Figure ??(f)), but a large scatter for the APG ones.
 366 When mixed variables are used (i.e. using τ_w , δ and U_e as shown in Figure ??(g)), which
 367 is commonly applied in existing WPS models, the low-frequency range collapses for the
 368 ZPG spectra only (see ZPG profiles shown separately in Figure ??(h)), but not for cases
 369 with strong APG, as p_{rms} does not scale with τ_w . On the other hand, normalisation based
 370 on outer variables only (i.e. using q_e , δ and U_e as shown in Figure ??(d)) gives a better
 371 collapse than that based purely on the inner variables; however, it still fails to collapse
 372 the low-frequency range. Based on these observations, the best ϕ_{pp} scaling among these
 373 options is thus $(\rho |\overline{u'v'}|_{\max})^2 \delta / U_e$.

374 The effects of Reynolds number (in combination with effects of APG) are analyzed
 375 next. Figures ??(a-c) categorize the wall-pressure PSDs in APG and ZPG flows into three
 376 Reynolds number groups: low- Re_θ ($Re_\theta \approx 300$ to 1000), mid- Re_θ ($Re_\theta \approx 2000$ to $8,000$)

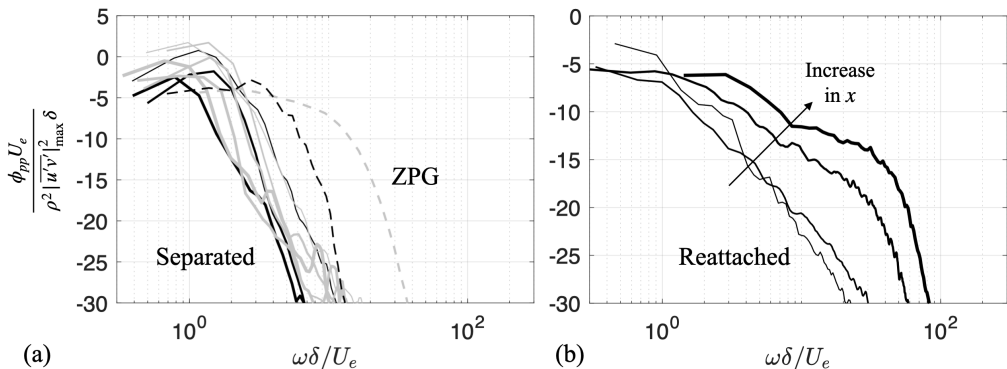


FIGURE 8. (a) Wall-pressure PSDs in separated-flow regions (—) compared to those at respective reference ZPG locations (---); gray lines show ? data at $x/\theta_o = 150, 175, 200, 220$ and 240 ; black lines show ? data at $x/\theta_o = 270, 300$ and 400 . (b) Wall-pressure PSDs in reattached-flow region of ? at $x/\theta_o = 275, 300, 350$ and 450 . In both (a) and (b), increase in line thickness indicates downstream direction.

377 and high- Re_θ ($Re_\theta \approx 8,000$ to $23,400$) groups. Note that in the high- Re_θ group, only
 378 ZPG or mild-APG flows are available in the present datasets. Figure ??(a) shows that
 379 all low- Re_θ spectra collapse well in the majority of frequency range. This is because the
 380 overlap range is limited and the low-frequency range is well collapsed by using $\rho |u'v'|_{\max}$
 381 as the pressure scaling. The CD-aerofoil data (---, ?) give high-frequency WPS levels
 382 that are slightly higher than the flat-plate data (—, ?) with matching Reynolds number
 383 and pressure gradients. The difference is attributed to the effects of surface curvature and
 384 the aerofoil trailing edge on the WPS, which is shown by Figure ??(a) to be relatively
 385 weak compared to the effects of the Reynolds number and pressure gradients. At higher
 386 Reynolds numbers, the overlap range appears and grows with Re_θ (Figures ??(b,c)). The
 387 width of the overlap range is shown to decrease with APG and the slope of this range
 388 becomes steeper with APG.

389 The PSDs in FPG flows are shown in Figure ??(d) using the two FPG datasets (in
 390 blue) of ? and ?, as compared to the corresponding ZPG spectra (in gray) from these
 391 two studies. Under $\beta \approx -0.5$, both spectra show a milder slope in the overlap range than
 392 the ZPG spectra. This is consistent with the steeper slope in APG flows discussed above.
 393 In addition, the overlap ranges are slightly widened under FPG with the low-frequency
 394 limit moving towards lower frequencies, especially for the lower-Reynolds-number case
 395 (?, blue circles). This is associated with a weaker mean-flow wake region under FPG.







Model	Legend
?	
?	
?	
?	
?	
Proposed model (introduced in Section ??)	

TABLE 4. List of WPS models examined with the present datasets.

396 To analyze the WPS associated with separated and reattached flows, Figures ??(a)
397 and ??(b) compare the spectra extracted, respectively, from the separated flow regions
398 and the regions downstream of the boundary-layer reattachment in the cases of ? and
399 ?. These two datasets are included as they are the only ones in the present collection
400 that include separated flows. Figures ??(a) shows that in the separated flow regions
401 both overlap-range and high-frequency wall-pressure fluctuations are reduced compared
402 to those in respective reference ZPG locations (dashed lines), due to the departure of
403 intense turbulent motions from the wall following the detachment of the shear layer.
404 The scaling does not collapse the low-frequency range as it does for attached flows.
405 This is expected as the wall pressure r.m.s does not scale with $|\overline{u'v'}|_{\max}$ in this region
406 (Figures ??(c)). However, it is interesting that the shape of the spectrum does not vary
407 significantly in the separated flow region: the spectra in Figures ??(a) all display a narrow
408 low-frequency peak with greatly reduced high-frequency contribution. This observation
409 provides insight to WPS modeling in separated flows, to be used in Section ??.

410 Downstream from the reattachment point, Figure ??(b) shows that the spectrum
411 recovers gradually from the low-frequency-dominant state inside the separated flow region
412 towards the equilibrium state, with augmented mid- to high-frequency contents.

413 5. Wall-pressure spectra modelling

414 5.1. Performance of existing wall-pressure spectra models

415 Most existing wall-pressure spectral models are developed for regions with zero and
416 adverse pressure gradients. Figure ?? compares a number of existing WPS models
417 introduced in Section ?? against the present datasets of ZPG and APG (attached

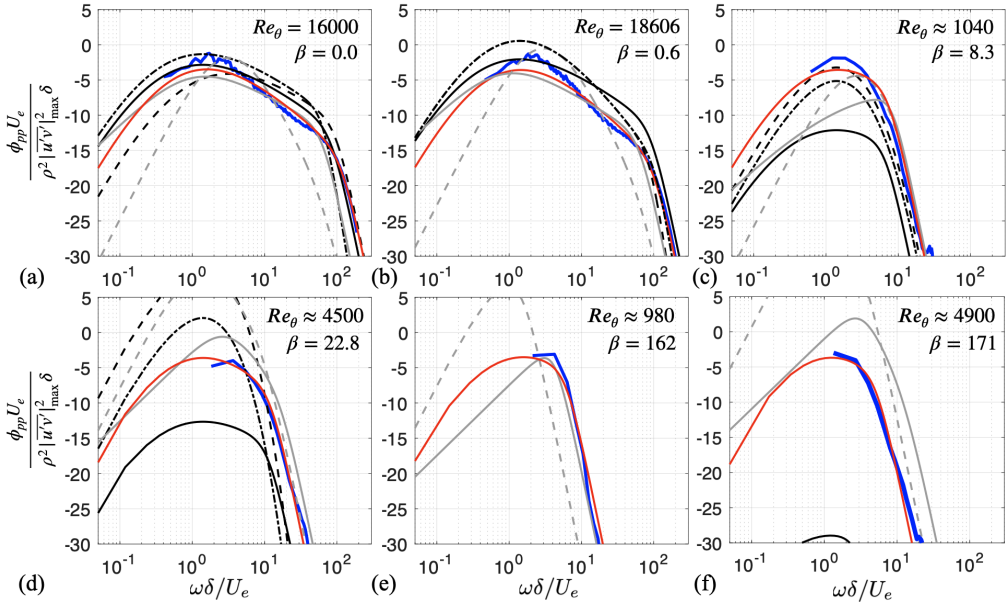


FIGURE 9. Comparison between predictions of WPS models and numerical or experimental measurements (—), for different types of flow: (a) ZPG, high- Re_θ flow ($?$, 2°), (b) weak-APG, high- Re_θ flow ($?$, 12°), (c) strong-APG, low- Re_θ flow ($?$), (d) very-strong-APG flow at intermediate Re_θ ($?$), (e) flow near separation point at a low Re_θ ($?$), and (f) flow near separation point at an intermediate Re_θ ($?$). Predictions of all models are re-normalized by $\rho|u'v'|_{\max}$, U_e and δ for comparison purposes. Legend of model results is given in Table ???. The proposed model (—) will be introduced in Section ???.

418 regions only) flows (marked by blue solid lines) for six different Re_θ - β combinations.
 419 Among them, Figures ??(e,f) show two examples near boundary-layer separation. The
 420 models and their legend are listed in Table ??, including a proposed model (shown
 421 by red solid lines) to be formulated in Section ?? to address the issues of the existing
 422 models observed in this section. All model predictions are re-normalised with the optimal
 423 ϕ_{pp} normalisation ($\rho|u'v'|_{\max}$, U_e and δ) identified in Section ???. The comparison of
 424 the measurement results among these six flows demonstrates dependencies of the WPS
 425 on the APG and the Reynolds number as discussed in Section ???. Under the present
 426 normalisation, the main variations are in the width and slope of the overlap range.

427 First, the overall performance of the WPS models in predicting the wall-pressure
 428 fluctuation intensity is analyzed based on the predicted p_{rms} value. Table ?? listed the
 429 prediction error of each of the tested model in the six flows examined in Figure ???. Good
 430 p_{rms} predictions (with errors up to 26%) were made by all models in the ZPG flow (row
 431 (a)). Under stronger APG (with β up to 23, rows (b) and (c)), over- or under-prediction

Model	Goody	Lee	Rozenberg	Hu	Kamruzzaman	Proposed model
(a) ZPG, high-Re	0.13	0.25	0.26	-0.20	-0.19	0.01
(b) Weak-APG, high-Re	0.25	0.40	0.40	-0.21	-0.07	0.00
(c) Strong-APG, low-Re	-0.64	-0.18	-0.34	-0.41	-0.13	-0.08
(d) Very-strong-APG, mid-Re	-0.61	2.00	0.33	0.49	1.89	0.05
(e) Near separation, low-Re	-0.99	-	-	-0.20	0.48	-0.08
(f) Near separation, mid-Re	-0.96	-	-	1.05	4.82	-0.02

TABLE 5. Wall-pressure r.m.s prediction errors from the existing models tested and the proposed models, examined for the six flows in Figure ???. The error is calculated as $(p_{rms} - p_{rms,a})/p_{rms,a}$, where $p_{rms,a}$ is the actual value from measurement. Rows (a-f) correspond to the flows in Figure ??(a-f), respectively. In (e) and (f), ? and ? models yield undefined values from double-precision floating-point number operations.

432 of a large fraction (40% to 60%) is seen in four out of the five existing models. However,
 433 in flows with very strong APG including the region near the separation point (rows (d)
 434 to (f)), very large errors are seen in all five existing models, as they were not formulated
 435 or calibrated for non-equilibrium strong-APG flows. The proposed model calibrated from
 436 some of these flows, on the other hand, is shown to reproduce very well the p_{rms} values
 437 (with up to 8% error) in all six flows. A good prediction of wall-pressure fluctuation
 438 intensity does not necessarily mean equally good prediction in the wall-pressure spectrum
 439 shape, which is analyzed next. The large model errors in rows (d) to (f) are also explained
 440 below.

441 In a ZPG flow (Figure ??(a)), almost all existing models (except ? model) give overall
 442 good predictions in the spectrum. For the weak-APG flow (Figure ??(b)), the tested
 443 models are shown to give reasonably good predictions overall. Goody's model over-
 444 predicts mid-to-high-frequency WPS content due to lack of sensitivities of the overlap-
 445 range width and slope to the pressure gradient. ? model does not produce an overlap range
 446 and, as a result, yields significantly under-predicted high-frequency contents. Moreover,
 447 except for ? model, all existing models give noticeable differences in the overlap-range
 448 slope from the experimental measurement.

449 For the flow under relatively weak APG ($\beta \approx 8$), Figure ??(c) shows that ? and
 450 ? models give very good overall predictions of the spectrum, whereas ? and ? models
 451 under-predict the WPS at low frequencies. ? model under-predicts the WPS in the whole

452 frequency range, which is expected, as this model was developed and calibrated for ZPG
 453 flows only.

454 In strong-APG flows (Figure ??(d-f)), especially near the boundary layer separation
 455 point, the existing models give large errors. This is because the model parameters used
 456 in these models: R_t and β , tend towards zero and infinity, respectively. Another source
 457 of error is the inappropriate pressure scaling (i.e. τ_w) used in the models. For instance,
 458 ? model:

$$\frac{\phi_{pp}(\omega)U_e}{\tau_w^2\delta^*} = \frac{0.78(1.8\Pi\beta + 6)(\omega\delta^*/U_e)^2}{[(\omega\delta^*/U_e)^{0.75} + C'_1]^{3.7} + [C'_3(\omega\delta^*/U_e)]^7}, \quad (5.1)$$

459 where $C'_3 = 3.76R_T^{-0.57}$, reaches a singularity as τ_w and R_t become zeros and β becomes
 460 infinity. Employing τ_w as the pressure scale for ϕ_{pp} also renders the dimensionless
 461 spectrum excessively sensitive to strong APGs, even if the flow stays attached. This issue
 462 is common in existing models. In addition, most of these models were fitted to limited
 463 types of flows, such as low-Reynolds-number aerofoil boundary layers in ?, flat-plate
 464 boundary layers in ?, and ZPG flows in ?. Moreover, sometimes the boundary layer flow
 465 properties used for model calibration were estimated from lower-fidelity methods such as
 466 XFOIL or RANS calculations, as opposed to DNS/LES or experimental measurements.
 467 In Section ??, these limitations are addressed to develop a well-behaved WPS model for
 468 both ZPG and APG flows, which can be attached or separated.

469 5.2. A new generalized WPS model for non-equilibrium boundary layers

470 In this section, a new wall-pressure spectral model is developed, with the ? model
 471 as a base. First, various components of the modification are introduced and justified.
 472 Then, prediction of the new model is compared to the datasets, in Figure ?? for attached
 473 APG flows and in Figures ?? to ?? for separated flows, reattached flows and FPG flows,
 474 respectively. Finally, a sensitivity analysis of the new model prediction to the model
 475 parameters is carried out, to verify that the intended dependencies are indeed captured.

476 The ? model is a good starting point as it has been shown successful in WPS
 477 prediction for ZPG boundary layers; it is also relatively simple compared to some other
 478 existing models. In summary, the ? model is modified by removing the Reynolds number
 479 parameter (R_t) and using model inputs that derive directly from the local mean velocity

distribution, $U^+(x, y)$. Only inputs that are quantifiable from engineering predictive approaches (such as RANS models) are considered, so the model is of practical use in engineering applications. The dependence of these inputs on the $U(y)$ distribution at a given x location allows the model to sense the local state of the turbulent boundary layer.

The ? model reads

$$\tilde{\phi}_{pp}(\tilde{\omega}) = \frac{a\tilde{\omega}^b}{(h\tilde{\omega}^c + d)^e + (f\mathcal{F}\tilde{\omega})^g}, \quad (5.2)$$

where $\tilde{\phi}_{pp} = \phi_{pp}/\phi_{pp}^*$ and $\tilde{\omega} = \omega/\omega^*$ are dimensionless WPS and frequency, respectively, based on a spectrum scale of ϕ_{pp}^* and a frequency scale of ω^* as listed in Table ???. The coefficients a to h and the function \mathcal{F} are defined in Table ??. The model was developed based on the observed dependencies of the low-frequency spectrum on the outer scales, as well as that of the high-frequency spectrum on the inner scales, in a ZPG or weak-pressure-gradient flow. The model was known to predict well the overlap range of the spectrum for ZPG boundary layers (as also shown in Figure ??(a)), which depends on the Reynolds number only. The dependence is captured by including R_t in the model. However, the overlap-range spectrum also depends on the pressure gradient in strong-pressure-gradient boundary layers. In Figure ??(a), the prediction of the original Goody's model is examined at several x locations of the ? case in the attached-flow region with weak to strong APGs. In this region, β ranges from 0 to 200 and Re_θ is from 2000 to 6000. With the increase in APG, Goody's model shows increasing under-prediction in the whole frequency range.

Table ?? listed the changes from the original ? model to the proposed model. The modified expressions of the model parameters were obtained by fitting a subset of the datasets: the APG and ZPG data of ?, ?, ?, ? and ?, as well as separated flow data of ? and ?. Datasets that were not used for model developing were used in testing the model in Figures ??(c,e,f) for attached APG flows, Figure ??(b) for a reattached flow, and Figure ??(b) for a FPG flow.

In the following, the main changes are introduced and progressively applied to demonstrate the improvement of each of them. First, the pressure scale (i.e. τ_w) on the left-

Parameters in Equation (??)	?	Present model
ϕ_{pp}^*	$(\tau_w^2 \delta)/U_e$	$[(\rho \overline{ u'v' })_{\max}]^2 \delta / U_e$
ω^*	U_e / δ	U_e / δ
a	3	3
b	2	2
c	0.75	$\min[1.0, 0.8 + (3.34 \times 10^{-4}) II^{1.86} (y_w^+)^{0.76}]$
d	0.5	0.7
e	3.7	3.7
f	1.1	1
g	7	7
h	1	1
\mathcal{F}	$R_t^{-0.57}$	$(y_w^+)^{-0.37}$
Separated flow ($\tau_w \leq 0$)		$y_w^+ = 2, c = 0.75, d = 0.5$
Limited-log-layer flow ($y_w^+ < 15$)		$y_w^+ = 15, c = 0.85$

TABLE 6. Comparison between ? model and the proposed model. ϕ_{pp}^* and ω^* are the chosen scalings for WPS and frequency, respectively. Special treatments for flow region characterized by a separated boundary layer or a limited logarithmic layer are listed.

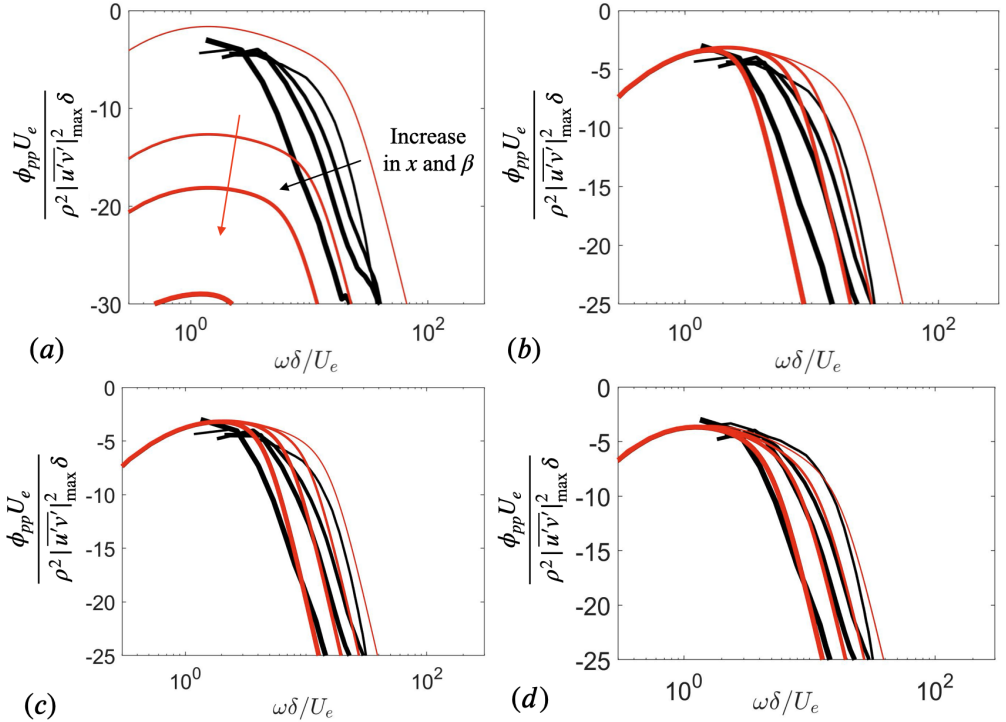


FIGURE 10. Comparison between model predictions of Equation (??) with progressive changes described in text (—) and ? (—) data in attached flows with weak to strong APGs, to show improvement brought by each model change. (a) ? model (predictions are plotted using the optimal normalisations), (b) pressure scale changed from τ_w to $\rho |u'v'|_{\max}$, (c) additionally replacing dependency on R_t with that on y_w^+ , (d) further addition of Coles' parameter. Thicker lines indicate increase in x (corresponding to increasing β).

508 hand-side of Equation (??) is replaced with $\rho|\overline{u'v'}|_{\max}$, with the additional change of
 509 replacing the constant $d = 0.5$ with 0.7 for a better low-frequency collapse with current
 510 data. The effect of these modifications is shown in Figure ??(b), where the low-frequency
 511 range is shown accurately predicted for all the x locations. The use of $\rho|\overline{u'v'}|_{\max}$ ensures
 512 that the spectral values are finite near the separation point.

513 Next, to capture the variation of overlap and high-frequency range in APG flows,
 514 a new parameter is needed to replace R_t to model the width change of the overlap
 515 range. Past studies showed that turbulent fluctuations in the logarithmic layer form the
 516 main contributor to the overlap range of the WPS. For example, ? showed that for ZPG
 517 boundary layers, with an increase in Reynolds number accompanied by a thickening of the
 518 logarithmic layer, the WPS overlap range becomes wider and its integral contribution to
 519 p_{rms}^2/τ_w^2 varies as $6.5+1.85 \ln(Re_\tau/333)$ at sufficiently high Reynolds numbers. Additional
 520 evidence in APG flows is provided by ?, who showed that the logarithmic layer yields
 521 the highest contribution to the overlap range of ϕ_{pp} based on analyses of the velocity
 522 sources of wall-pressure Poisson's equation. Here, a new model input is introduced: $y_w^+(x)$,
 523 defined as the local elevation of the upper edge of the logarithmic layer, to sensitize the
 524 model spectrum to the change in logarithmic layer thickness due to Reynolds number
 525 and/or pressure gradients. The subscript w in y_w represents the width of the logarithmic
 526 layer. Specifically, the term $1.1R_t^{-0.57}$ is replaced with $(y_w^+)^{-0.37}$. The new expression is
 527 obtained by assuming a power function of y_w^+ and performing a non-linear least square
 528 fit (using both ZPG and APG datasets) to calculate the exponent.

529 The parameter $y_w^+(x)$ is dynamically determined based on the boundary layer mean
 530 velocity $U(x, y) = \bar{u}$, as the y^+ location where $U^+(x, y) - [\kappa(x)^{-1} \log y^+ + B(x)]$ departs
 531 from 0 at the upper limit of the logarithmic layer (as shown in Figure ??(c)). Here, κ
 532 is the von Kármán constant and B is the log-law intercept, both of which allowed to
 533 vary along x in a non-equilibrium boundary layer. Note that due to the use of local
 534 viscous scaled units in y_w^+ and U^+ , etc., the present modification needs special treatment
 535 at the separation point and inside the separated flow region, which will be discussed
 536 later. To determine $\kappa(x)$, the diagnostic function $I(x, y) = y^+ \partial U^+ / \partial y^+$ (Figure ??(b))
 537 is calculated from the mean velocity profile (Figure ??(a)) for data of ?. The local minima

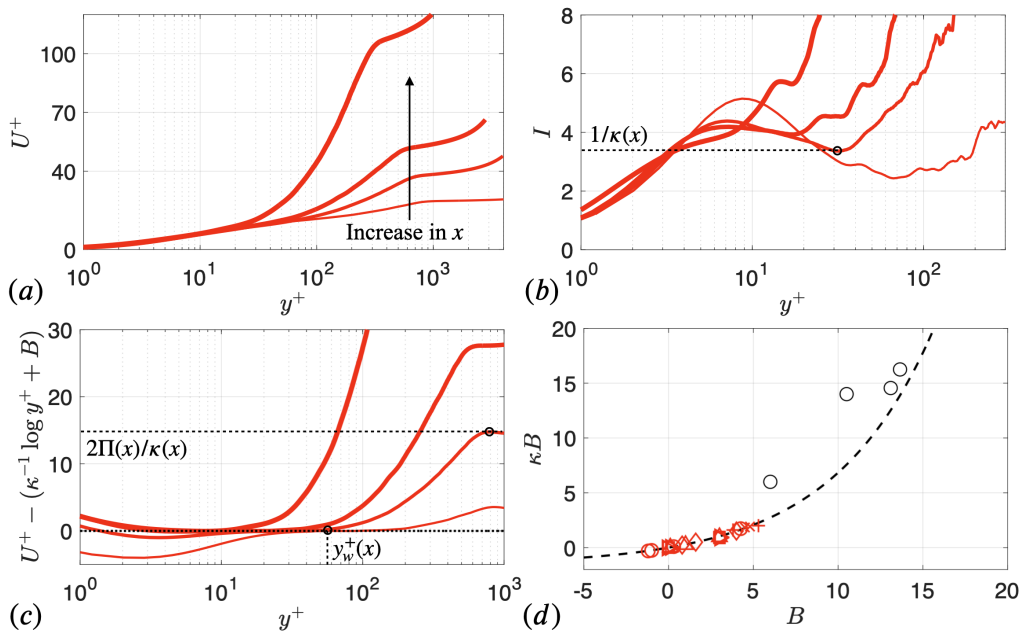


FIGURE 11. (a-c) Calculation of $\kappa(x)$, $B(x)$ and model parameters shown using ? data at locations $x/\theta_o = 50, 105, 120$ and 130 . Increasing line thickness indicates increase in x . (a) Mean velocity profiles in inner units. (b) Diagnostic function, $I = y^+ \partial U^+ / \partial y^+$. (c) Velocity profiles with logarithmic relation subtracted. Calculations of κ , Π and y_w^+ are indicated for $x/\theta_o = 105$ in (b,c). (d) Correlation between calculated κB and B , compared to the fitted relation from ? (---): \circ ? (attached flow before separation), \circ ? (attached flow downstream of reattachment), \diamond ?, \times ?, $+$?, \square ?, \triangleright ? and \triangle ?.

538 of $I(x, y)$ at a given x is taken as $1/\kappa(x)$. Following the determination of $\kappa(x)$, $B(x)$ is
 539 calculated using $U^+(x, y) - [\kappa(x)^{-1} \log y^+ + B(x)] = 0$. Figure ??(d) shows that the
 540 correlation between $\kappa(x)$ and $B(x)$ obtained for all cases in the present attached-flow
 541 datasets is consistent with that observed by ? from a large collection of flows with or
 542 without pressure gradients. As shown in Figure ??(c) compared to Figure??(b), the
 543 modeling of overlap-range width based on y_w^+ is successful for the present APG datasets:
 544 the high-frequency range is now better predicted with the corrected width. As the APG
 545 becomes stronger, y_w^+ decreases as shown in Figure ??(c), reducing the overlap-range
 546 width as shown in figure ??(c). The main WPS prediction error is now predominantly
 547 an inaccurate slope of the overlap range, as shown in Figure ??(c).

548 The change in WPS overlap-range slope (in addition to the change of the width of this
 549 range as is characterized by y_w^+) is assumed to be caused by the variation in the strength
 550 of the outer-layer turbulent motions. This assumption arises from the understanding that

551 an APG leads to more energized large turbulence motions in the outer layer and a thinner
 552 logarithmic layer. In addition, an APG is known to cause an increase in low-frequency
 553 WPS contents and a decrease in mid-to-high-frequency ones (e.g. ???), which is reflected
 554 in a steeper overlap-range slope. To account for the variation in the strength of the wake
 555 region, an additional model input is used: Coles' parameter, $\Pi(x)$. An augmentation of Π
 556 signals stronger turbulent intensity and mixing in the outer layer. Here, $\Pi(x)$ is evaluated
 557 based on $U^+(x, y)$, by measuring the peak value of $U^+ - [\kappa^{-1}(\log(y^+) + B)]$ (as shown
 558 in Figure ??(c)) and dividing it by $2/\kappa(x)$. In the generic model form in Equation (??),
 559 the coefficient c is known to impose the slope of the overlap range of ϕ_{pp} (???). The
 560 present datasets suggest that c is a function of both y_w^+ and Π : for flows with larger y_w^+
 561 values, the same pressure gradient difference leads to a larger slope variation compared
 562 to cases with smaller y_w^+ values. Therefore, the constant c is replaced by a function of
 563 both Π and y_w^+ . A posynomial functional form is assumed; the constant coefficients and
 564 exponents are fitted based on the present datasets. Additionally, for boundary layers with
 565 very strong APG or near the separation point, the logarithmic layer diminishes and the
 566 WPS overlap range is very narrow or absent. At these flow locations the modelled WPS
 567 is weakly sensitive to the c value. The present datasets yield a maximum value of $c \approx 0.98$
 568 in strong-APG flows. For simplicity, c is capped at 1.0. This treatment, however, may
 569 be improved in the future when more high-Reynolds-number strong-APG data become
 570 available. The final form of the generalized WPS model is

$$\frac{\phi_{pp}(\omega)U_e}{(\rho|u'v'|_{\max})^2\delta} = \frac{3(\omega\delta/U_e)^2}{[(\omega\delta/U_e)^c + 0.7]^{3.7} + [(y_w^+)^{-0.37}(\omega\delta/U_e)]^7}, \quad \text{where} \quad (5.3)$$

571

$$c = \min [1.0, 0.8 + 3.34 \times 10^{-4} \Pi^{1.86} (y_w^+)^{0.76}]. \quad (5.4)$$

572 For the ZPG flow shown in Figure ??(a), the ? model and the proposed model give
 573 similar predictions and both compare well with the experimental measurements. The
 574 small difference between the predictions of the two models is because of the use of different
 575 model parameters and that the fitting of the proposed model is conducted for both ZPG
 576 and APG flows. For the strong-APG flows in the present datasets, Figure ??(d) and
 577 Figure ?? show that the generalized model predicts the WPS very well. Note, however,

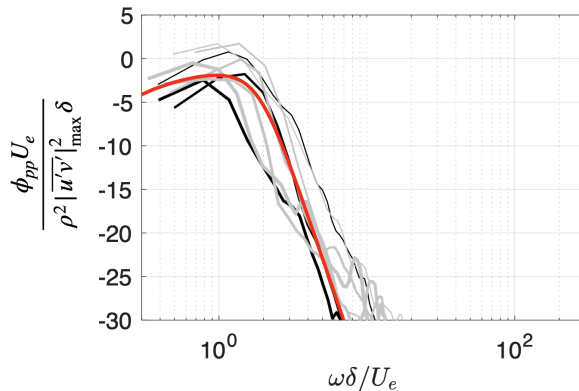


FIGURE 12. Comparison between model prediction (—) and simulation data (— and —) in the separated-flow regions. Increasing line thickness indicates an increase in x values as used in Figure ??(a).

578 that the present strong-APG data used to calibrate this model are from limited-Reynolds-
 579 number flows with a rather narrow WPS overlap range. Additional data from high-
 580 Reynolds-number strong-APG flows are not available, but are needed to validate the use
 581 of the model of its present form in flows with higher Reynolds numbers.

582 A few scenarios require special treatments as listed in Table ?. For cases with very
 583 low Reynolds numbers and extreme adverse pressure gradients, which practically removes
 584 the logarithmic region from the boundary layer (i.e. if $y_w^+ < 15$), y_w^+ and c are set to
 585 constant values: $y_w^+ = 15$ and $c = 0.85$ as calibrated from the present datasets, to reflect
 586 the insensitivity of ϕ_{pp} to either Reynolds number or pressure gradient as shown in
 587 Figure ??(a). Moreover, in case of boundary layer separation, modification of the model
 588 is needed for x locations at the separation point and inside the separation bubble. Inspired
 589 by the similar WPS profiles across the normalized frequency range in the separated region
 590 as shown in Figure ??(b), y_w^+ and c are set to constants: $y_w^+ = 2$, $c = 0.75$, and d is set to
 591 0.5 (Table ?), calibrated based on the data of ? and ?. The separation modification is
 592 activated for x regions where $C_f(x)$ is calculated as zero or negative, corresponding to the
 593 region of mean-flow separation. With the aforementioned separated-flow treatment, the
 594 proposed model is evaluated at a number of streamwise locations inside the separation
 595 regions of the flows of ? and ? in Figure ?. The WPS prediction does not vary with x
 596 in this region, since the model parameters are set to constants. Overall good comparison
 597 with the simulation data is achieved. Although the separation treatment introduces a

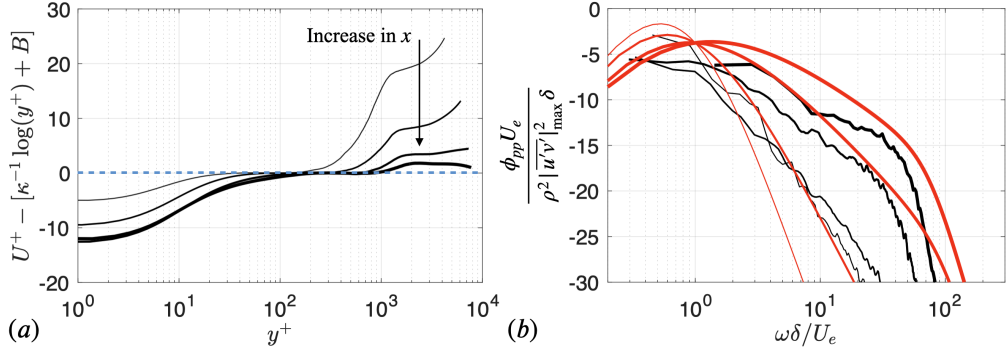


FIGURE 13. Comparison between model prediction (—) and ? data (—) in the attached-flow region downstream of reattachment point (at x/θ_o from 250 to 350, the most downstream location corresponding to near equilibrium flow). (a) Mean velocity profiles with the logarithmic relation subtracted; --- value corresponding to logarithmic layer. (b) Wall-pressure PSD comparison. Increasing line thickness indicates an increase in x .

598 discontinuity in c value at the separation point (as c approaches 1 towards the point
 599 while $c = 0.75$ at that point), it is shown not to affect the prediction significantly, as the
 600 overlap range is short in the strong-APG region in the vicinity of the detachment.

601 Although the model is primarily developed for attached or separated APG flows, it is
 602 examined in other regions of a non-equilibrium boundary layer to explore its extendibility
 603 to more universal applications. First, the model is evaluated in the region downstream
 604 from the flow reattachment point till a near-equilibrium ZPG state in Figure ?? against
 605 ? data, at four x locations between $x/\theta_o = 250$ and $x/\theta_o = 350$. Figure ??(a) shows
 606 that, near the reattachment point (shown by the thinnest lines), the local mean velocity
 607 departs significantly from a canonical boundary layer profile, without a clear logarithmic
 608 layer. With increasing x , the logarithmic layer gradually recovers towards the equilibrium
 609 ZPG state and the overlap range of the WPS thickens gradually (Figure ?? (b)). The
 610 model is shown to capture such trend of WPS variation. The overall spectral levels are
 611 well predicted due to the approximate scaling of p_{rms} on $\rho|\overline{u'v'}|_{\max}$, while the spectral
 612 shape is captured by $y_w^+(x)$ and $\Pi(x)$ representing the local thickening of the logarithmic
 613 layer and the weakening of wake, respectively, during recovery.

614 In addition, the model is tested in FPG flows as shown in Figure ??, against the
 615 experimental data of ? and ?. Figure ??(a) shows that, under FPGs (shown in blue) as
 616 compared to the ZPG profiles (shown in gray), the main change is a reduction of Π ,
 617 which leads to a milder slope of the WPS overlap range. Figure ??(b) shows that this

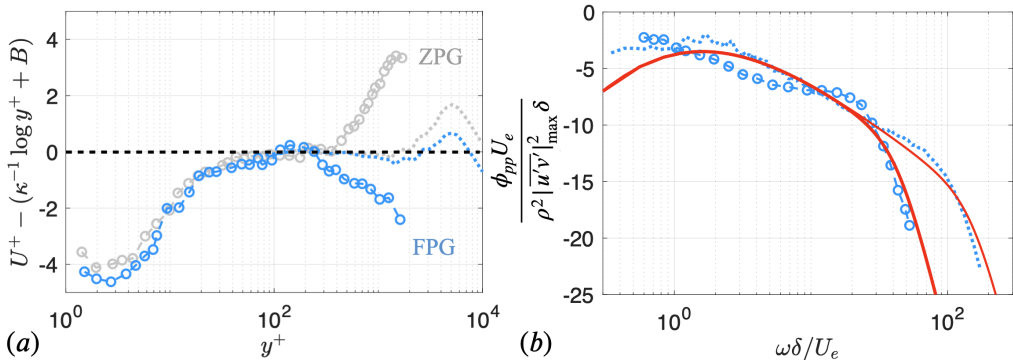


FIGURE 14. Comparison between model prediction (—) and experimental data in FPG flows: \circ ?, $\beta = -0.5$ and \circ ?, $\beta = -0.5$. (a) Mean velocity profile with the logarithmic relation subtracted; the ZPG profile in each of the two studies (shown in gray) is compared. --- Value corresponding to logarithmic layer. (b) Wall-pressure PSD comparison.

618 change in WPS is globally captured well by the proposed model.

619 Figure ?? shows results of sensitivity analyses carried out for the parameters y_w^+
 620 and Π of the proposed model. The WPS predictions obtained with $\pm 30\%$ change of
 621 each of the two parameters (marked by the highlighted region) are compared with
 622 the datasets, for three types of flows with different ranges of Reynolds number and
 623 β . Figures ??(a,c,e) show that the variation of y_w^+ has an effect on the overlap-range
 624 and high-frequency contents, by controlling the width of the overlap range. The effect
 625 appears to be particularly strong in a weak-APG flow. Figures ??(b,d,f) show that $\Pi(x)$
 626 modifies the slope of the overlap range, with the model particularly sensitive to its value
 627 in high-Reynolds-number flows where the overlap range is pronounced. These results
 628 show that the introduced parameters affect the WPS prediction in their intended ways.
 629 Furthermore, slight variations in quantifying y_w^+ and Π do not significantly worsen WPS
 630 prediction.

631 6. Conclusions and discussions

632 In this study, datasets collected from numerical (DNS and LES) and experimental
 633 studies are used to characterize the variation of wall-pressure statistics in various types
 634 of boundary layer flows, attached or separated and then reattached, with zero, adverse or
 635 favorable pressure gradients at different ranges of Reynolds number. These data were used
 636 to gain insight for developing a new WPS model and to test it. Only existing datasets

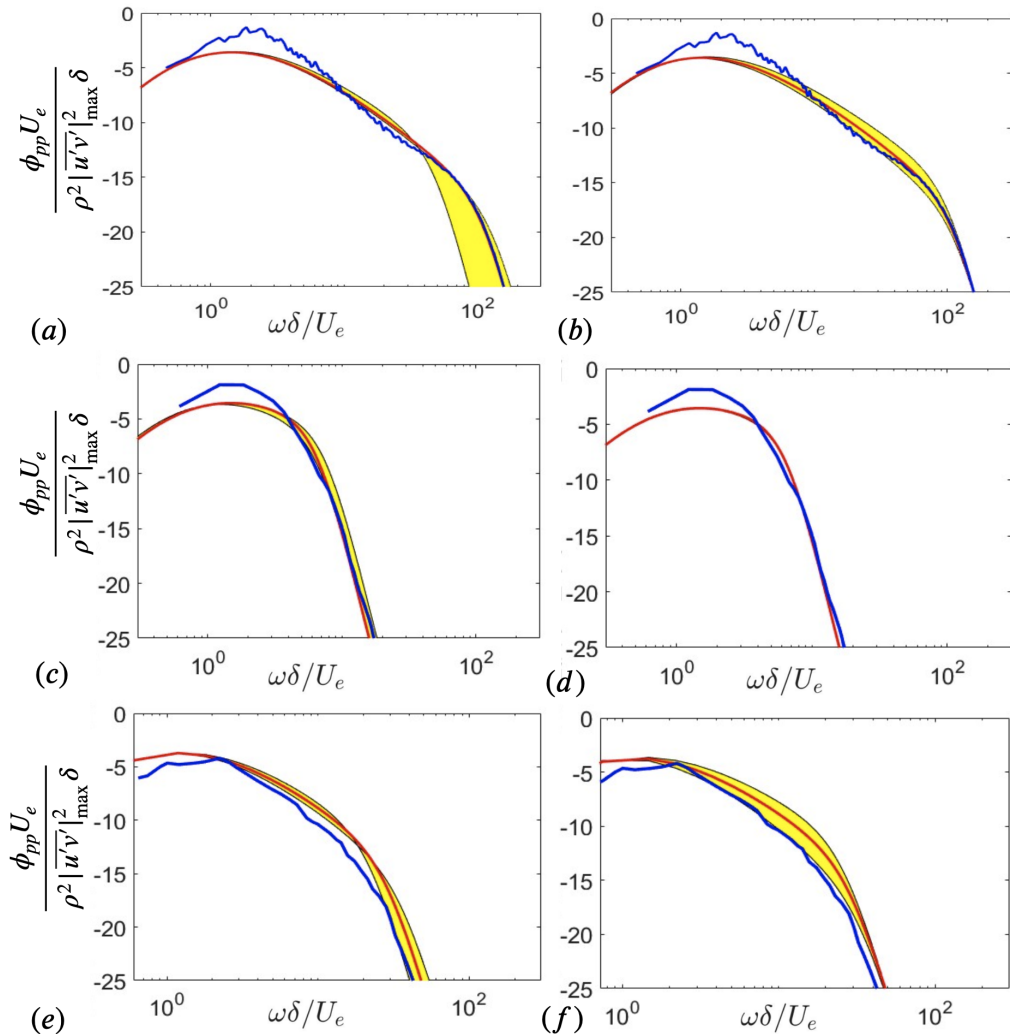


FIGURE 15. WPS prediction of the proposed model (—) compared to measurements (—) in the following cases: (a,b) high-Reynolds-number and weak-APG flow ($\beta = 0.58$), (c,d) low-Reynolds-number and strong-APG flow ($\beta = 8.3$), and (e,f) high-Reynolds-number and strong-APG flow ($\beta = 6$). Yellow regions mark prediction variations with $\pm 30\%$ change in input parameters y_w^+ (a,c,e) or II (b,d,f). In (d), variation of II does not change WPS prediction as c is set to a constant at this location due to $y_w^+ < 15$ (see Table ??).

637 that contain both WPS data and wall-normal profiles of the mean velocity measured
 638 at the same streamwise locations as the WPS are considered, as these quantities are
 639 required in testing the new model. For non-zero pressure-gradient flow data, the present
 640 focus is on non-equilibrium ones. The numerical data in the datasets were validated
 641 in various flow quantities. They are not prone to errors originating from installation
 642 effects as in many experimental studies and are free from modeling errors as in RANS or

643 boundary layer closures used in the development of some existing WPS models. Strongly
 644 non-equilibrium streamwise pressure gradient variations are included in the datasets. By
 645 comparing different sets of variables used to normalize the wall-pressure spectrum (ϕ_{pp}),
 646 an optimal set of scales is identified: U_e , δ and $\rho|\overline{u'v'}|_{\max}$, and is used for wall-pressure
 647 spectrum model development.

648 The performances of various existing wall-pressure spectral models are evaluated in
 649 the flows contained in the datasets. These models are shown to fail to predict the wall-
 650 pressure spectra in non-equilibrium strong-APG flows. The failures are caused by the
 651 use of inappropriate pressure scaling (τ_w), being fitted to limited types of flows, and the
 652 dependencies on u_τ -based model parameters, as u_τ reduces to zero at the detachment
 653 point.

654 Next, more robust model parameters are proposed and used to modify Goody's model.
 655 These parameters are (i) the logarithmic-layer extent, y_w^+ , and (ii) Coles' parameter, II .
 656 These parameters carry information on the local state of the boundary layer flow as
 657 found in the mean velocity profile. The parameters, together with the scaling variable
 658 $\rho|\overline{u'v'}|_{\max}$, are quantifiable or inferable from turbulence models (e.g. Reynolds-averaged
 659 Navier-Stokes (RANS) models) or experimental measurements of the mean velocity and
 660 wall friction. For APG-flow experiments where the Reynolds shear stress is not directly
 661 measured, the present datasets suggest that $\rho|\overline{u'v'}|_{\max}(x)$ may be approximated based
 662 on the wall shear stress at an upstream ZPG location. Using y_w^+ and II is a more direct
 663 approach to model the change in contributions from wall-layer and outer-layer turbulent
 664 flows to the wall-pressure spectrum, compared to existing approaches based on local
 665 pressure gradient (e.g. Clauser's parameter, β) and/or local Reynolds number (e.g. R_t).
 666 As the streamwise development of the mean velocity contains the history effect of non-
 667 equilibrium pressure gradients, y_w^+ and II are measures of this history effect. In contrast,
 668 the history effect of pressure gradient is not directly represented by a local pressure
 669 gradient parameter, such as β which is used in some existing WPS models.

670 Comparison with available numerical and experimental measurements shows that the
 671 proposed model gives good predictions for ZPG, APG (attached-flow region) and FPG
 672 flows. For the two datasets with strong APGs and boundary-layer separation considered

673 herein, the wall-pressure spectra are shown to display similar shapes and magnitudes
674 across the separation bubble. There, the model is shown to give overall good predictions,
675 if the overlap-range width and slope are set to constants fitted based on present data.
676 More separated flow data are needed to test this model, for example, in flows with various
677 separation-bubble sizes and dynamics.

678 A qualitatively good prediction is also obtained downstream of flow reattachment
679 where the boundary layer departs significantly from its equilibrium state. Hence, the
680 new model is considered as a generalized wall-pressure spectral model for a wide range
681 of ZPG/weak-pressure-gradient and non-equilibrium, strong-pressure-gradient boundary
682 layers, as opposed to existing models designed for limited types of flows.

683 In practice, the accuracy of the proposed model used with measured inputs (e.g. from
684 experiments or RANS simulations) depends on the accuracy of the measured quantities,
685 including mean velocity, wall friction and (modeled or inferred) Reynolds shear stress.
686 For example, RANS simulations may not be accurate in predicting the wall shear stress,
687 separation point or the separation bubble extent in an APG flow. However, this is a
688 limitation for WPS models in general; improving turbulence closures or experimental
689 measurements in non-equilibrium boundary layers is an important, but separate, topic.
690 The main contributions of this work are (i) to ensure WPS model boundedness in non-
691 equilibrium APG flows and (ii) to include local velocity-based variables to better model
692 the history effect of pressure gradients on the wall-pressure spectrum.

693 **Acknowledgments**

694 SP is grateful for the funding provided by the Consortium for the Development of
695 Ultra-High Efficiency Quiet Fans at Université de Sherbrooke. SP and JY also gratefully
696 acknowledge the additional financial support by Office of Naval Research (Award No.
697 N00014-17-1-2102). Computational support was provided by Michigan State University's
698 Institute for Cyber-Enabled Research and the Digital Research Alliance of Canada.

699 **Declaration of interests**

700 The authors report no conflict of interest.